Communications in Physics, Vol. 31, No. 4 (2021), pp. 361-368
DOI:https://doi.org/10.15625/0868-3166/15916

ONE-STEP HYDROTHERMAL SYNTHESIS AND PHOTOCATALYTIC ACTIVITY OF SnO_2/rGO NANOCOMPOSITES: EFFECTS OF PH VALUES

PHAM VAN TUAN†, HOANG BA TUONG[2] AND TRAN NGOC KHIEM[1]

[1]*International Training Institute for Materials Science,*
Hanoi University of Science and Technology, No.1 Dai Co Viet, Hanoi, Vietnam
[2]*School of Chemical Engineering,*
Hanoi University of Science and Technology, No. 1 Dai Co Viet, Hanoi, Vietnam

E-mail: †tuan.phamvan@hust.edu.vn

Received 7 March 2021
Accepted for publication 14 April 2021
Published 02 September 2021

Abstract. *In this study, tin oxide /reduced graphene oxide (SnO_2/rGO) samples were prepared by hydrothermal method. The structural characteristics, phase composition, morphology and size of the samples were studied by X-ray diffraction, Raman scattering spectroscopy, and scanning electron microscopy, respectively. Results showed that SnO_2 nanoparticles were formed in the tetragonal rutile crystal structure with a size ranging from 4.65 nm to 5.77 nm when the pH was increased from 5 to 9. The morphology of SnO_2 nanoparticle together with rGO layers was observed in the FESEM image of these samples. The absorption spectra of SnO_2/rGO samples showed the characteristic absorption peak of SnO_2 at 296 nm, in which the band gap value of the material decreased from 3.91 eV to 3.81 eV when pH was increased from 5 to 9. The simultaneous formation of the two phases of SnO_2 and rGO was demonstrated by Raman scattering spectroscopy. The best photocatalytic efficiency of SnO_2/rGO reached 86% after 90 min under visible light irradiation for the samples prepared at pH = 7.*

Keywords: SnO_2/rGO nanocomposites; pH value; photocatalytic activity.

Classification numbers: 81.16.Hc; 72.20.Jv; 81.05.ue.

I. INTRODUCTION

Environmental pollution is becoming increasingly alarming [1]. Scientists have discovered many approaches to treat the environment, including photocatalysis, which has many advantages,

such as cheap, clean, and energy-saving operations [1, 2]. In this technique, photocatalytic materials are used to decompose environmental pollutants under visible-light, ultraviolet, or solar radiation [1,3,4]. In photocatalytic materials, metal oxides, such as SnO_2, TiO_2, and ZnO [1,5–8], are widely used to degrade environmental pollutants.

Tin oxide (SnO_2) is an n-type semiconducting material with a wide band gap (˜3.6 eV) and a tetragonal rutile crystalline structure [2, 8–10]. SnO_2 has a more positive valence band and stronger oxidizing capacity than TiO_2 [11]. However, the disadvantage of SnO_2 is that it only works with ultraviolet light because of the large band gap [11]. Attempts have been made to improve the photocatalytic capacity of SnO_2 under visible light [3, 4]. To improve the photocatalytic ability of SnO_2, researchers have doped SnO_2 with other elements [12] or combined it with other materials with narrow band gap [9, 13]. Among these materials, graphene is a new material with many unique properties [14]. Graphene can efficiently absorb visible light, has high charge-carrier mobility, and high specific surface area [14]. When the photogenerated carriers are generated, these electrons and holes move in two different directions due to a different charge mobility, inhibiting the recombination of charge carriers and separate photogenerated electrons and holes [14]. Many types of photocatalytic materials containing graphene such as TiO_2/graphene [15, 16], ZnO/graphene [17, 18], and SnO_2/graphene [4, 14] have been used to improve the photocatalytic efficiency. Among these materials, SnO_2/graphene has many unique properties and has good photocatalytic efficiency [14, 19–21]. Furthermore, the photocatalytic efficiency of SnO_2/graphene depends on the fabrication conditions including synthesis method, and the ratio of the initial precursors [13,20–22]. Among these parameters, pH influences the structure and photocatalytic efficiency of SnO_2/rGO nanomaterials.

SnO_2/rGO nanomaterials are fabricated using different methods, such as the microwave-assisted hydrothermal method [14], photochemical method [23], melamine template [3], hydrothermal method [13, 22], and sol-gel process [24]. Among these methods, the hydrothermal method has valuable advantages, such as low reaction temperature, simple equipment, energy saving, low cost, and environmental friendliness [22].

In this work, SnO_2/rGO was fabricated using the hydrothermal method. The effect of pH on the structure, composition, morphology, size, and photocatalytic properties was studied.

II. EXPERIMENT

II.1. Materials

The chemicals (from Merck) used to synthesize SnO_2/rGO material were tin (IV) chloride pentahydrate ($\geq$98%, $SnCl_4.5H_2O$), sodium hydroxide (reagent grade, $\geq$98%, NaOH), ethanol ($\geq$99%, C_2H_2OH), and graphene oxide powder (15–20 sheets, 4%–10% edge-oxidized, GO). All chemicals were used without further purification.

II.2. Preparation of SnO_2/rGO nanocomposites

SnO_2/rGO nanocomposites were synthesized using the hydrothermal method as previously described [13,22]. In the typical process, 2.3 g of $SnCl_4.5H_2O$ was dissolved in 20 ml of deionized water for 30 min to obtain $SnCl_4$ solution. Exactly 1.06 g of NaOH was dissolved in 20 ml of deionized water for 30 min to obtain NaOH solution. NaOH solution was gradually added into the $SnCl_4$ solution, and the solution was stirred for 30 min to obtain a precipitate mixture. The pH value was changed by the ratio of NaOH and $SnCl_4$. The pH values investigated were set to

5, 7, and 9. An appropriate amount of GO was added into the mixture, which was stirred for 30 min. Then, 30 ml of C_2H_5OH was added to the above mixture. The final mixture was transferred to a Teflon-lined stainless-steel autoclave, and the solution was heated at 180˚C for 24 h. After the hydrothermal process, the sample was washed with deionized water and ethanol. Finally, the sample was air-dried at 90˚C for 24 h.

II.3. Characterization of SnO_2/rGO nanocomposites

The crystal structure and phase of the samples were analyzed on a D5000 X-ray diffractometer (XRD) (Siemens, Germany) with a CuKα radiation source (λ = 0.15406 nm) and Raman scattering (inVia Raman Microscope, Renishaw, UK) with laser excitation at 633 nm. The surface morphology of the samples was studied using an S-4800 field emission scanning electron microscope (FESEM) (Hitachi, Japan). The UV-Vis absorption spectrum (a V-650 UV–vis spectrophotometer, Jasco, USA) was used to investigate the absorbance properties of the materials.

II.4. Investigation of the photocatalytic properties of the SnO_2/rGO nanocomposites

The photocatalytic activity of the SnO_2/rGO nanocomposites was examined via decomposition of the methylene blue (MB) under visible light (under a normal 60-W filament lamp at a distance of 10 cm). MB was dissolved in deionized water by using a magnetic stirrer for 1 h with a resulting concentration of 1 μg/mL. SnO_2/rGO nanocomposites (8 mg) were dispersed into MB solution (30 ml) via ultrasonic vibration for 30 min and stirred in the dark for 1 h to achieve adsorption–desorption equilibrium. This solution was illuminated with visible light at different times. After illumination, the solution was centrifuged, and UV-vis absorption spectrometry was conducted to investigate the photocatalytic decomposition.

III. RESULTS AND DISCUSSION

Figure 1(a) shows the XRD patterns of SnO_2/rGO samples at different pH values. The XRD patterns show diffraction peaks corresponding to 2θ angles of 26.7˚, 33.8˚, 38.0˚, 51.6˚, 54.8˚, 57.9˚, 61.8˚, 65.2˚, 71.2˚, and 78.5°. These diffraction peaks belong to (110), (101), (200), (211), (220), (002), (310), (301), (202), and (321) planes of the tetragonal rutile structure of SnO_2 (JCPDS card No 41-1445) [13,19,22,25]. The diffraction peaks of rGO were not observed in the X-ray diffraction pattern. This finding is possibly associated with the overlap of the peak (002) of the rGO with the peak (100) of SnO_2 and the low concentration and intensity of rGO [19,22,23]. When the pH value increased from 5 to 9, the position of the diffraction peaks did not change, but their intensity changed remarkably. The diffraction peak intensity at pH = 7 value was the largest. This result shows that the crystallinity of SnO_2 samples prepared at pH = 7 is the best. The chemical composition analysis of GO prior to reduction obtained from the energy dispersive X-ray (EDX) patterns is shown in Fig. 1(b). The results show that GO consists of two elements C and O. C accounts for 93.37 atomic%, and O accounts for 6.63%. This result is consistent with the data provided by Merck Company (graphene oxide powder, 15–20 sheets, 4%–10% edge-oxidized, code: 796034).

The crystallite size of the SnO_2 nanoparticles in the samples was calculated using Scherrer equation $D = 0.9\lambda/(\beta\cos\theta)$ [26] where λ is the X-ray wavelength (0.15406 nm), θ is the diffraction peak Bragg angle, and β is the FWHM. Table 1 shows that in the pH range of 5 to 9, the SnO_2 nanoparticle size increased from 4.65 nm to 5.77 nm.

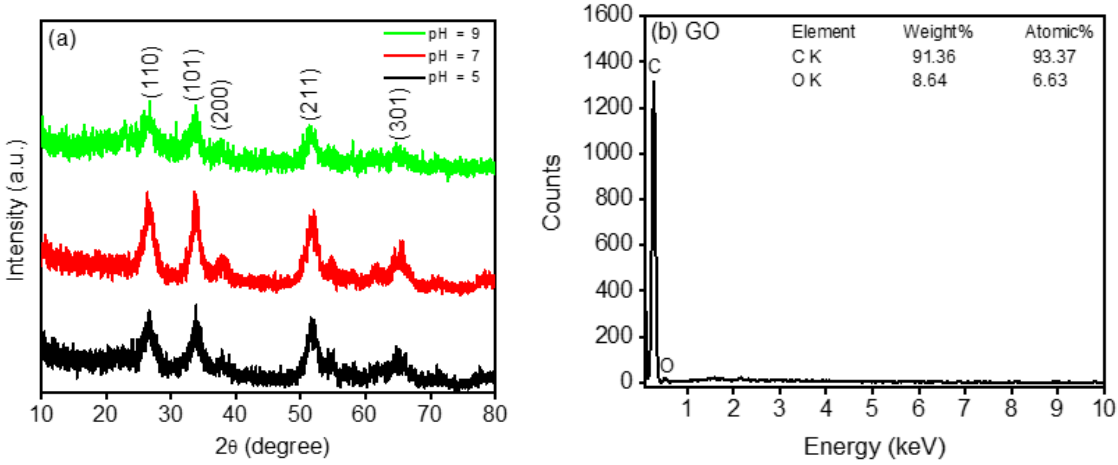

Fig. 1. (a) XRD patterns of SnO_2/rGO at different pH values, and (b) EDX analysis of GO before reduction.

Table 1. Dependence of SnO_2 particle size on pH values.

Samples	Planes	2θ (°)	FWHM (°)	Crystallite size (nm)	Average crystallite size (nm)
SnO_2/rGO (pH = 5)	(110)	26.53	1.84	4.63	4.65
	(101)	33.79	1.66	5.23	
	(211)	51.83	2.26	4.08	
SnO_2/rGO (pH = 7)	(110)	26.53	1.83	4.66	4.94
	(101)	33.81	1.50	5.78	
	(211)	51.74	2.11	4.37	
SnO_2/rGO (pH = 9)	(110)	26.52	1.63	5.23	5.77
	(101)	33.68	1.33	6.52	
	(211)	51.68	1.66	5.56	

Figure 2 shows the FESEM images of SnO_2/rGO samples prepared at different pH values. The results showed that the SnO_2 nanoparticles with size from 4 to 12 nm were surrounded by the rGO layers. Nanoparticles have spherical shape and its size do not change remarkably according to the pH value. The morphology of SnO_2 nanoparticles did not change with pH. In these samples, other morphologies such as nanorods, nanowires, and nanoflowers were not observed. Simultaneous observation of both SnO_2 and rGO nanoparticles showed that SnO_2/rGO nanomaterials were successfully fabricated using the hydrothermal method.

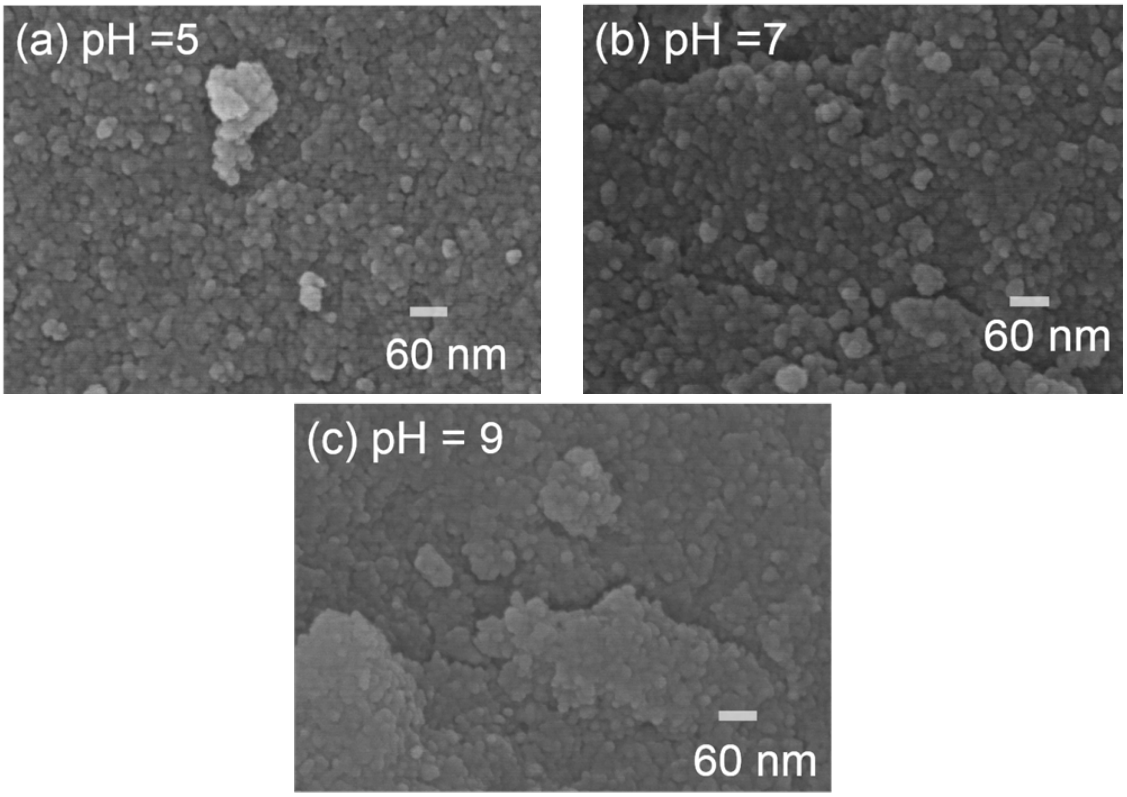

Fig. 2. FESEM images of SnO_2/rGO nanocomposites with different pH values.

Figure 3 shows the Raman spectra of SnO_2/rGO prepared at different pH values. The Raman scattering spectra of SnO_2/rGO showed peaks at 352, 564, 627, 766, 1332, and 1583 cm^{-1}. The scattering spectral peaks of SnO_2/rGO clearly show the characteristic peaks of SnO_2 and rGO materials. The spectral peaks of SnO_2 correspond to the observed peaks at 564, 627, and 766 cm^{-1} [10,22,23], which are assigned to the S, A_{1g}, and B_{2g} vibration modes, respectively [10]. The Raman peaks of graphene correspond to the detected peaks at 1332 and 1583 cm^{-1} [10,22,23]. The peak at 1332 cm^{-1} corresponding to the D band of graphene is

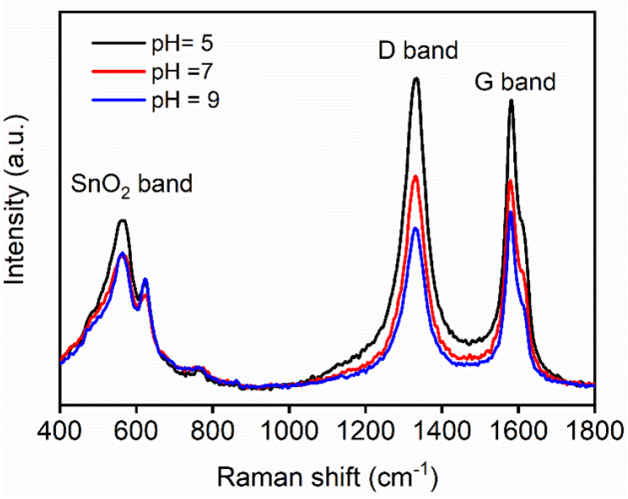

Fig. 3. Raman scattering spectra of SnO_2/rGO with different pH values.

involved in defects in the carbon lattice [10,22,23]. The peak at 1583 cm^{-1} corresponding to the G band of graphene is involved in the vibration of sp^2 hybridized carbon atoms [10,22]. When pH was increased from 5 to 9, the I_D/I_G ratio decreased. Hence, the reduction of GO to rGO decreases when the pH value increases from 5 to 9. The Raman results show the simultaneous appearance of the SnO_2 and rGO peaks, indicating that the SnO_2/rGO nanomaterials were prepared successfully by using the hydrothermal method.

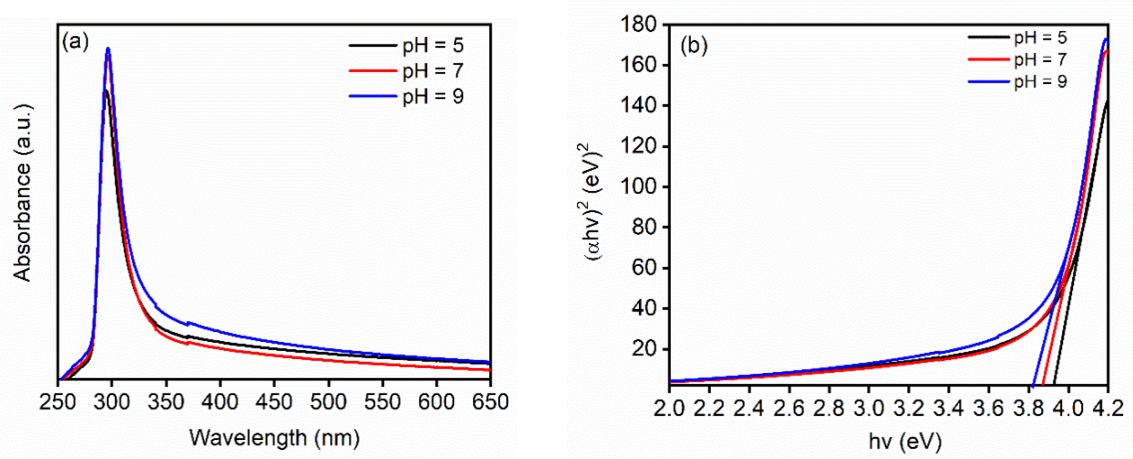

Fig. 4. (a) UV-vis absorption spectra, and (b) plots of $(\alpha h\nu)^2$ versus energy (hν) of SnO_2/rGO with different pH values.

Figure 4 (a) shows the UV-vis absorption spectra of SnO_2/rGO prepared at different pH values. The results showed that the absorption spectra of the samples exhibited a peak at 296 nm. This peak is related to the characteristic absorption of SnO_2 [10]. When the pH value changed, the absorption peak position did not change, and the absorption of the samples at pH = 7 and 9 is the best. Fig. 4 (b) shows the plot of $(\alpha\ h\nu)^2$ versus (hν), which was used to calculate the band gap energy (E_g). The E_g value of SnO_2 nanoparticles in SnO_2/rGO nanocomposite was calculated using the formula: $\alpha\ (h\nu) = K\ (h\nu - E_g)^{1/2}$ [27], where E_g is the band gap energy, hν is the incident photon energy, K is a constant, and α is the absorption coefficient. The results showed that the band gap energy values were 3.91, 3.84, and 3.81 eV for samples at pH = 5, 7, and 9. Thus, the band gap energy decreased from 3.91 eV to 3.81 eV when the pH value increased from 5 to 9.

Figures 5 (a, b, and c) show the absorption spectra of MB after photocatalytic treatment using SnO_2/rGO nanoparticles prepared at different pH values. Results showed that the absorption spectrum of MB consisted of one peak at 664 nm and one shoulder at 613 nm [3, 22]. In all the samples, under the illumination of light, the absorption peak of the MB decreased sharply. Therefore, the concentration of MB was significantly reduced after the photocatalytic reaction. For an effective understanding of the photocatalytic efficiency of the samples, the C/C_0 was plotted versus irradiation time, as shown in Fig. 5(d). The results showed that MB decreased by 83.5%, 86%, and 76.3% for samples at pH = 5, 7, and 9, respectively. The results showed that at pH = 7, the photodegradation efficiency of SnO_2/rGO to decompose MB under visible light is the best.

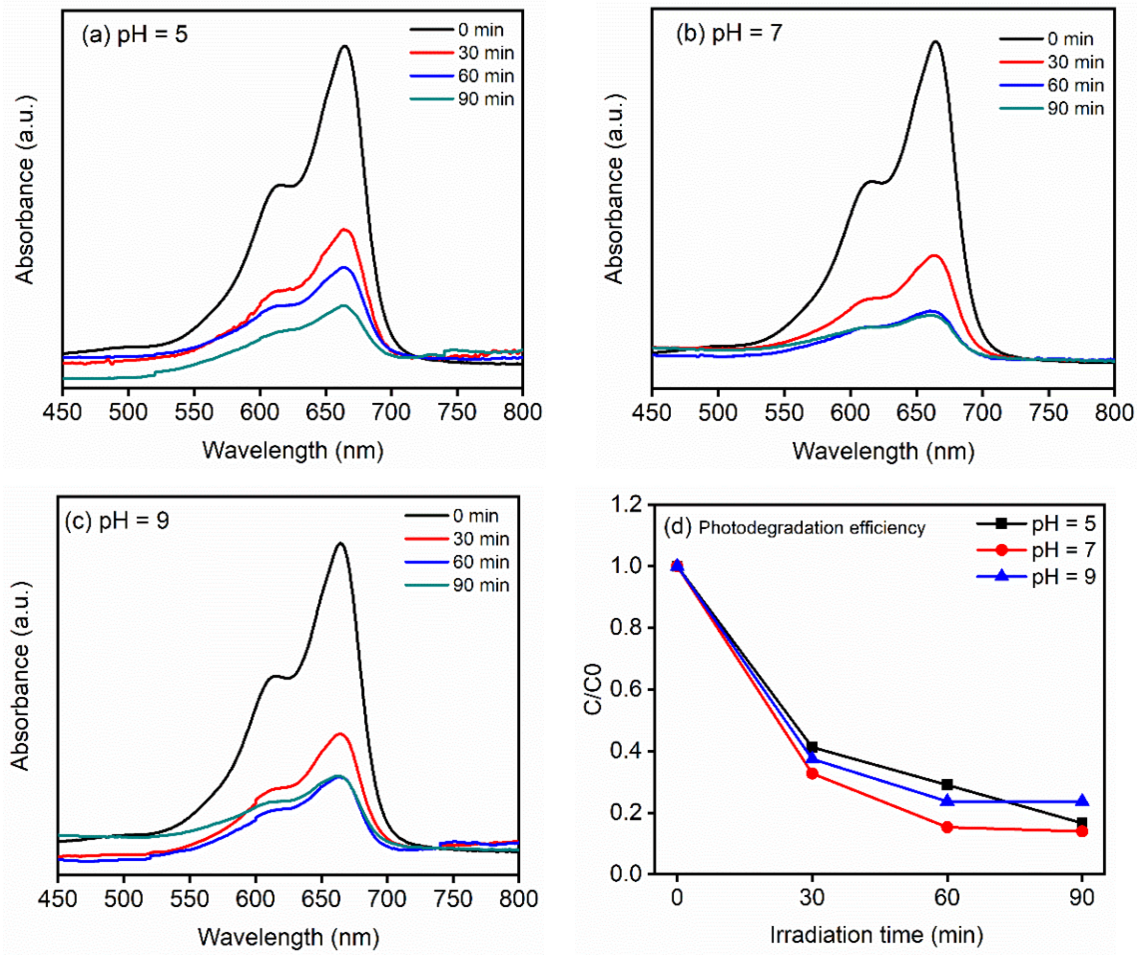

Fig. 5. (a, b, c) Time-dependent absorption spectra of MB solutions containing SnO_2/rGO nanocomposite samples obtained via visible-light irradiation and (d) Photodegradation efficiency of SnO_2/rGO nanocomposite samples.

IV. CONCLUSIONS

In the present study, SnO_2/rGO nanocomposites were successfully prepared using the hydrothermal method at different pH values. The obtained results showed that the SnO_2/rGO nanomaterials exhibited the morphology of SnO_2 nanoparticles with sizes ranging from 4.65 nm to 5.77 nm surrounded by the rGO layers. The SnO_2/rGO material possessed a characteristic absorption peak of SnO_2 at 296 nm, and the E_g value decreased from 3.91 to 3.81 when the pH increased from 5 to 9. Raman scattering spectra demonstrated that SnO_2 and rGO coexisted in a nanocomposite material, where the reduction of GO to rGO decreased when the pH value increased from 5 to 9. The best photocatalytic efficiency of SnO_2/rGO reached 86% after 90 min under visible light irradiation for the samples prepared at pH = 7.

ACKNOWLEDGEMENTS

This research is funded by Vietnam National Foundation for Science and Technology Development (NAFOSTED) under grant number 103.02-2018.25.

REFERENCES

[1] Z. Chen, G. E. Chen, H. Y. Xie, Z. L. Xu, Y. J. Li, J. J. Wan, L. J. Liu, H. F. Mao, *Sep. Purif. Technol*. **259** (2021) 118184.
[2] R. Shyamala, L. Gomathi Devi, *Chem. Phys. Lett*. **748** (2020) 137385.
[3] X. Hong, R. Wang, S. Li, J. Fu, L. Chen, X. Wang, *J. Alloys Compd.* **816** (2020) 152550.
[4] R. Pandiyan, S. Mahalingam, Y.H. Ahn, *J. Photochem. Photobiol. B Biol.* **191** (2019) 18.
[5] X. Zhang, J. Chen, M. Wen, H. Pan, S. Shen, *Phys. B Condens. Matter*. **602** (2021) 412545.
[6] H. Mahmood, M.A. Khan, B. Mohuddin, T. Iqbal, *Mater. Sci. Eng. B Solid-State Mater. Adv. Technol.* **258** (2020) 114568.
[7] C. Ademola Bode-Aluko, O. Pereao, H. H. Kyaw, L. Al-Naamani, M.Z. Al-Abri, M. Tay Zar Myint, A. Rossouw, O. Fatoba, L. Petrik, S. Dobretsov, *Mater. Sci. Eng. B Solid-State Mater. Adv. Technol.* **264** (2021) 114913.
[8] Y. C. Chang, J. C. Lin, S. Y. Chen, L. Y. Hung, Y. R. Lin, C. Y. Chen, *Mater. Res. Bull.* **100** (2018) 429.
[9] X. Ni, C. Chen, Q. Wang, Z. Li, *Chem. Phys*. **525** (2019) 110398.
[10] A. Mallik, I. Roy, D. Chalapathi, C. Narayana, T.D. Das, A. Bhattacharya, S. Bera, S. Bhattacharya, S. De, B. Das, D. Chattopadhyay, *Mater. Sci. Eng. B Solid-State Mater. Adv. Technol.* **264** (2021) 114938.
[11] W. Ben Haj Othmen, A. Hamdi, A. Addad, B. Sieber, H. Elhouichet, S. Szunerits, R. Boukherroub, *J. Photochem. Photobiol. A Chem*. **367** (2018) 145.
[12] B. Babu, A. N. Kadam, R. V. S. S. N. Ravikumar, C. Byon, *J. Alloys Compd.* **703** (2017) 330.
[13] V. T. Pham, H. Le Trung, N. K. Tran, H. Chu Manh, H. Nguyen Duc, H. Tran Thi Quynh, T. H. Pham, *Mater. Res. Express*. **5** (2018) 095506.
[14] C. Aydın, *J. Alloys Compd*. **771** (2019) 964.
[15] D. M. Tobaldi, D. Dvoranová, L. Lajaunie, N. Rozman, B. Figueiredo, M. P. Seabra, A. S. Škapin, J. J. Calvino, V. Brezová, J. A. Labrincha, *Chem. Eng. J*. **405** (2021).
[16] D. Li, J. Sun, T. Shen, H. Song, J. Liu, C. Wang, X. Wang, R. Zhao, *J. Solid State Chem*. **286** (2020) 121301.
[17] P. Van Tuan, T.T. Phuong, V.T. Tan, S.X. Nguyen, T.N. Khiem, *Mater. Sci. Semicond. Process*. **115** (2020) 105114.
[18] M. Qiang, H. Xiaomin, L. Ke, D. Rui, H. Zhang, X. Bo, Z. Kewen, *Sep. Purif. Technol*. **259** (2021).
[19] H. Liu, T. Liu, X. Dong, Y. Lv, Z. Zhu, *Mater. Lett.* **126** (2014) 36.
[20] L. Tang, V. H. Nguyen, Y. R. Lee, J. Kim, J.-J. Shim, *Synth. Met*. **201** (2015) 54.
[21] Y. Xie, S. Yu, Y. Zhong, Q. Zhang, Y. Zhou, *Appl. Surf. Sci.* **448** (2018) 655.
[22] P. Van Tuan, L. T. Hieu, C. M. Hoang, H. B. Tuong, V. T. Tan, T. T. Q. Hoa, N. X. Sang, T. N. Khiem, *Nanotechnology* **32** (2021) 015201.
[23] Y. Chen, F. Sun, Z. Huang, H. Chen, Z. Zhuang, Z. Pan, J. Long, F. Gu, *Appl. Catal. B Environ.* **215** (2017) 8.
[24] T. Tajima, H. Goto, M. Nishi, T. Ohkubo, Y. Nishina, H. Miyake, Y. Takaguchi, *Mater. Chem. Phys.* **212** (2018) 149.
[25] H. Chen, X. Pu, M. Gu, J. Zhu, L. Cheng, *Ceram. Int*. **42** (2016) 17717.
[26] B. D. Cullity, *Elements of X-ray diffraction*, 2nd edition, Addison-Wesley Publ. Co. Read. MA. (1978) 100-105,277-279.
[27] J. Tauc, *Mater. Res. Bull.* **3** (1968) 37.